Modular quadrupole array capture line for plasma-accelerated electrons

Bruno D. Muratori, Deepa Angal-Kalinin, Alexander R. Bainbridge, Joe Crone, Clive Hill, James K. Jones, Hywel L. Owen, Thomas H. Pacey, Yuri M. Saveliev, and Neil R. Thompson

UKRI-STFC Daresbury Laboratory, Warrington, United Kingdom and The Cockcroft Institute, Sci-Tech Daresbury, Warrington, United Kingdom

Daniel Symes, Nicolas Bourgeois, and Oliver Finlay

UKRI-STFC Rutherford Appleton Laboratory, Didcot, United Kingdom

(Received 4 July 2025; accepted 19 March 2026; published 7 May 2026)

The UK Extreme Photonics Applications Centre (EPAC) intends to flexibly provide laser-accelerated GeV-scale electrons to a wide array of experiments and like other such facilities must efficiently capture them from a laser-wakefield acceleration (LWFA) source. Here we describe a unique, modular beam capture optics system based on a FODO array of Halbach permanent-magnet quadrupoles and show how that modular arrangement can be used in different configurations to provide energy-selected and focused bunches for different purposes. We present an engineering concept for the beamline that incorporates diagnostics and drive laser extraction and describe the effect of field errors and misalignments and their mitigation.

DOI: 10.1103/8hns-3zqp

I. THE EXTREME PHOTONICS APPLICATIONS CENTRE

The plasma arising when a gas target is ionized by an intense laser pulse can develop very large electric fields exceeding 10 GV/m, 2 to 3 orders of magnitude greater than those commonly obtained in conventional radio-frequency (rf) cavities used in particle accelerators today. The high accelerating gradient offered by such a scheme has long been recognized as an attractive means of generating the electrons required for applications that include colliders for fundamental particle physics; generation of intense x-rays in a free-electron laser or from an inverse Compton source; secondary sources (e.g., bremsstrahlung) that may be used in industrial imaging; and applications in medical imaging and radiotherapy.

The UK Extreme Photonics Applications Centre (EPAC) is a national laser facility under construction at STFC's Rutherford Appleton Laboratory that will generate pulsed, narrow-band (percent-level energy spread) electron bunches using the laser wakefield acceleration (LWFA) mechanism [1], delivering tunable GeV-scale mean kinetic energies. The laser driving the acceleration in the gas target is based on the DiPOLE concept [2] and will deliver approximately 1 PW peak laser power at a repetition rate of 10 Hz [3]; this corresponds to a pulse output energy of 30 J and a duration of < 30 fs. The laser will be focused to a spot size of around 50 μm ($1/e^2$ radius), providing an intensity $> 10^{18}$ W cm^{-2}. Two of the three eventual experimental areas in EPAC will be commissioned initially: Experimental area 1 (EA1) has a fixed laser configuration delivering a long-focus beamline; Experimental area 2 (EA2) contains a large, flexible-configuration vacuum chamber with short-, medium and long-focus options. Here, we discuss how EA1 will incorporate a novel electron transport beamline.

LWFA produces high-brightness electron bunches with a small source size (of order μm), and with comparable bunch charge (around 100 pC) and emittance (of order mm mrad) to a conventional rf cavity photoinjector. However, the source divergence of LWFA bunches is much larger (mrad scale) [1,4–6] and must be effectively captured by magnetic focusing components (or their equivalent) placed close to the LWFA source exit. An additional complexity at EPAC is the requirement to flexibly deliver bunches for different applications; this means the ability to focus differing-energy bunches at multiple locations within the EA1 experimental area, up to the maximum distance of 20 m from the LWFA source that is presently available.

The electron energy produced at the LWFA source will be tunable by varying the laser and target conditions [7,8] and typically will be above 1 GeV. Experiments with PW-class laser drivers have demonstrated maximum energies up

Published by the American Physical Society under the terms of the Creative Commons Attribution 4.0 International license. Further distribution of this work must maintain attribution to the author(s) and the published article's title, journal citation, and DOI.

to 10 GeV [9–11] and the EPAC facility has been designed with this in mind.

In this study, we consider a beam-conditioning channel for a 1 GeV design energy, using electron bunch properties predicted by a particle-in-cell (PIC) simulation of the laser-gas interaction. Our modular approach can be adapted for the higher energies expected as EPAC develops and may also be applicable to other high-energy facilities such as ELI [12] and EuPRAXIA [13].

For the initial electron bunch capture—placed immediately downstream of the plasma—we will utilize a permanent-magnet quadrupole (PMQ) array. PMQs are typically small and relatively inexpensive and achieve a reasonable field quality [14–19]. They can readily provide the strong transverse field gradients that are required to capture large-divergence LWFA-produced electrons: much in excess of 100 T/m. As we discuss below, we need at least 350 T/m PMQs, which in turn limits the free aperture within them to perhaps 10 mm diameter or less; however, this does not limit beam transmission due to the small initial beam size and emittance. In some situations, EPAC will use active plasma lenses, which can in principle produce gradients up to about 3000 T/m [20]; we have considered conventional magnets (electromagnetic and permanent-magnet) for the present work due to the much greater existing experience using them in beamlines.

To accommodate changes in the mean electron energy, one option is to use quadrupoles with a variable gradient such as the zero power tunable optics (ZEPTO) [21,22] or quadrupole permanent magnet with variable gradient (QUAPEVA) [23] PMQ designs. However, these have limitations on the maximum gradient they can obtain and are significantly more expensive than similar-strength fixed-gradient PMQs; they are also less suitable for the higher-energy bunches that may be later generated at EPAC.

Instead, in this report, we propose the use of a modular FODO (focusing-defocusing) array composed of fixed-strength PMQs of the Halbach type, where FODO "blocks" can be added or removed depending on the experimental conditions required by EPAC users. The key novelty here is that the conditioning of the electrons takes place over several FODO pairs, rather than by using a conventional triplet arrangement. The PMQ array can be used as a stand-alone element to create a point-to-point focus within the LWFA source chamber (at approximately 1 m distance from the source) or as the first component in a multistage electron beamline that provides a variable interaction point either for diagnostic measurements or experimental applications further downstream in the experimental area.

II. CAPTURE ARRAY DESIGN

A. Modular, gradual focusing

Many LWFA sources use a (fixed strength) PMQ triplet where the first element is placed very close to the plasma source to minimize beam size growth and consequent beam loss [24–26]; in some schemes, the quadrupole strengths are asymmetric, and in general, they are intended for a single, fixed mean electron energy. A modular FODO array achieves the same outcome of a point-to-point focus of a bunch through interleaving F and D quadrupoles, such that the overall phase advance between source and focus is still π in each transverse plane. Interleaving the F and D elements reduces the large divergence in one plane if strong focusing is applied first in the other plane and thereby limits beam size growth and loss. This, in turn, allows a sufficiently large bandwidth of electrons to be transmitted, albeit with some intrinsic chromaticity that varies the focal position with energy.

Putting the PMQs in modular groups on movers offers another advantage in that the array can be flexibly reconfigured—for example, by removing some quadrupoles entirely from the electron path—to provide bunch capture at different central energies or to produce a focal spot at a different distance from the source. Figure 1—based on the parameters given in Table I—illustrates the principle of a FODO array and shows how the horizontal and vertical beam sizes are progressively controlled over a number of FODO periods. The FODO array beam-optical transfer matrix is effectively acting as a single, long lens with roughly equal focusing strength in either plane, with the largest transverse beam size half-way through that lens. Another advantage of using identical F/D PMQs is that an F-quadrupole can be reconfigured to be a D-quadrupole simply by rotating it 90° on its mounting plate. While a

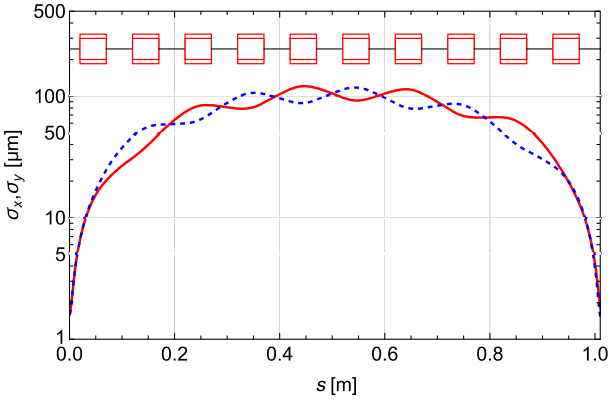


FIG. 1. Illustration of how the electron rms Transverse beam sizes vary through a FODO capture array for an example 1 GeV LWFA-generated electron bunch (σ_x in red/solid, σ_y in blue/dashed); a representative initial beam waist at the plasma exit is assumed of $\beta_x = \beta_y = 5$ mm and a normalized emittance of $\epsilon_N = 1$ μm, corresponding to an initial electron source size of $\sigma = 1.6\,\mu$m. A single 500 T/m quadrupole of 50 mm length is insufficient to focus in a given plane, but an interleaved array of 500 T/m quadrupoles (shown here) progressively captures in both planes without unduly large transverse beam size being generated in either plane. Here, the 1 GeV electron bunch is brought to a focus 1 m from the source.

TABLE I. Main parameters for the 1 GeV FODO array design shown in Fig. 1.

Halbach FODO array:	
Number of quadrupoles	10
Quadrupole length	50 mm
Quadrupole strength	500 T/m
Quadrupole separation	50 mm
Quadrupole aperture (radius)	4 mm
Focal spot distance	1 m

FODO array naturally provides a single point-to-point focus, it may also be used to couple into a conventional beamline once the initial large LWFA divergence has been conditioned; the downstream beamline elements may then be composed of conventional electromagnetic quadrupoles (EMQs).

B. Variables relevant in capture array design

Assuming the F/D elements are symmetrically arranged, we may vary three parameters while keeping the overall point-to-point focusing condition: quadrupole gradient; quadrupole length; inter-quadrupole separation. In doing so, while keeping the integrated gradient constant, one would expect that higher-gradient, shorter quadrupoles would give a smaller maximum bunch size at the FODO array center; this is illustrated in Fig. 2. As shown later, a reasonable trade-off between gradient and aperture requirements is to specify a PMQ gradient around 500 T/m so that

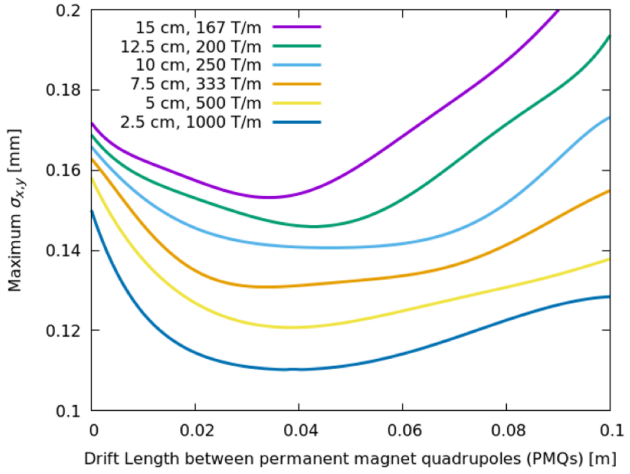


FIG. 2. Maximum beam size (1σ values) midway through a ten-quadrupole array as quadrupole gradient, length and inter-quadrupole separation are varied, while keeping the integrated strength the same. Here, the same 1 GeV initial electron bunch parameters are used as in Table I. As one would expect, a larger gradient restricts the maximum transverse beam size generated halfway along the array. This behavior would also hold for electromagnetic quadrupoles, which would, however, be limited to lower gradients.

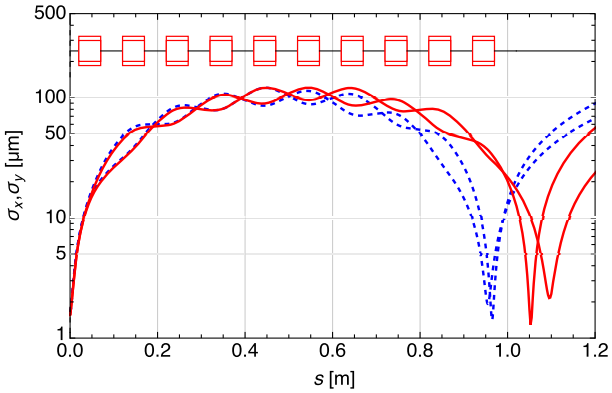


FIG. 3. Using the same ten-quadrupole FODO array as that shown in Fig. 1 but with initial electron energy variation of ±5%. We show the transverse beam sizes for 0.95 GeV (blue, dashed) and 1.05 GeV (red, solid). The focal plane distance from the LWFA source varies by around the same percentage.

sufficient beam transmission can be achieved; a 5 cm separation between quadrupoles allows for collimation, diagnostic instrumentation, and other components such as a plasma mirror between the first two quadrupoles, which separates out the laser pulse that initially copropagates from the LWFA source parallel to the generated electrons.

An obvious question is what happens in a FODO array if the electron energy or divergence changes from its nominal value, which would be expected in today's LWFA sources. Using a reasonable variation in mean energy of ±5% [1] (which we predict for our LWFA source), Fig. 3 shows what we would intuitively expect: higher-energy bunches have a longer focal length. Similarly, if we double the initial divergence, the maximum transverse beam size also doubles. Both phenomena naturally arise with a fixed beam-optical system.

C. Varying the electron energy in EPAC

A feature of our FODO array design—based on a common quadrupole block—is that it can be readily reconfigured for higher electron energies. Individual quadrupoles can be combined into focusing structures composed of multiple elements of the same polarity to achieve stronger focusing; for example, an FF-DD-FF… doublet scheme or even a triplet FFF-DDD-FFF… may be used to minimize the number of quadrupoles required for a given energy. For example, a 5 GeV scheme composed of 21 quadrupoles can be used to bring the beam to a focus less than 2.5 m from the LWFA source (see Fig. 4).

III. THE CAPTURE ARRAY

A. Halbach quadrupoles

The capture concept described above benefits from having quadrupoles with as high a gradient as can practicably be achieved provided sufficient aperture is available

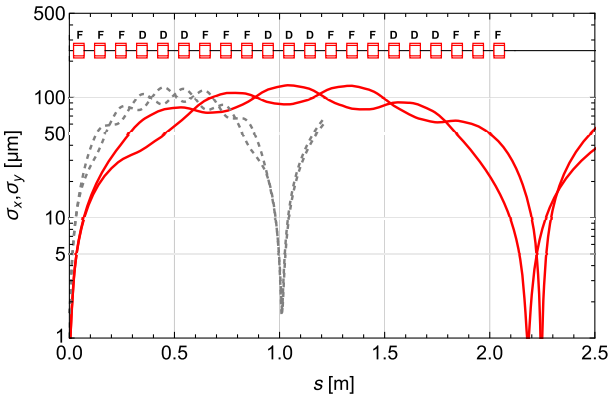


FIG. 4. Example FODO array for 5 GeV focusing; here a 3.5 FODO composed of 500 T/m PMQs—in the arrangement FFF-DDD-FFF-DDD…—brings a 5 GeV bunch to a focus less than 2.5 m from the LWFA source, with a maximum transverse beam size comparable to the 1 GeV configuration (Fig. 1, beam size evolution here shown for comparison gray, dashed).

to give good beam transmission. The transmission and error analysis later in this paper justifies the choice of a 4 mm internal quadrupole clear radius, with an assumption that all the capture quadrupoles are used in vacuum so that a central beam pipe can be avoided. The later analysis also shows a requirement that the quadrupoles achieve the same integrated gradient as each other to around 1% accuracy; this is somewhat better than the 2% magnetization variation often observed in permanent-magnet blocks, and so we here propose a novel tuning-pin method to trim individual quadrupoles to match their gradients.

The required specification of the quadrupoles is given in Table II. Preliminary magnet modeling in Opera-2D [27] indicated that a Halbach design could provide the required gradient and good gradient region with a 4 mm inscribed radius. However, for ease of alignment during construction, it was decided to increase the magnetic radius to 4.5 mm and add an internal stainless-steel retaining pipe of internal radius 4.0 mm. This small increase in magnetic radius means that the external radius of the magnet blocks needs to be doubled to maintain the same on-axis gradient. A first tolerance study of the Halbach design—using typical manufacturing errors in block dimensions of ±50 μm, remanent field errors of ±2%, and magnetization angle errors of ±2°—indicated that the gradient variation among the quadrupoles would exceed the specification of 1%.

TABLE II. Halbach PM quadrupole specification.

Peak gradient	≈500 T/m
Maximum length	50 mm
Integrated gradient	25 T
Internal radius	4 mm
1% good gradient radius	≈2 mm
Peak gradient variation	1% full range

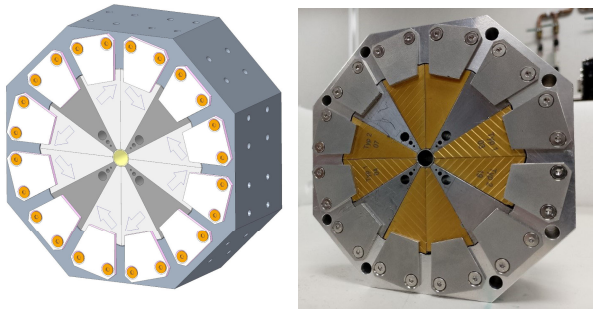


FIG. 5. Hybrid Halbach permanent-magnet tunable quadrupole for the EPAC capture array. Left: the eight lighter-colored segments show indicatively the magnetization directions; in the four darker-colored steel poles can be seen the tuning holes into which steel rods may be inserted. Right: assembled Halbach quadrupole. Blocks are inserted from the side shown, using the indexing holes that are visible at the outer frame perimeter; the blocks are later retained with clamp plates. The three-bit tuning holes are visible in the four steel poles.

B. A novel tunable Halbach design

A hybrid design has been chosen as shown in Fig. 5. Those blocks in which the magnetic field would be oriented radially—referred to here as the "poles"—were replaced with 1006 magnetic steel. This allows the required gradient to be achieved with an acceptable outer magnetic radius of 46 mm, and also allows us to trim the field within those steel poles.

To trim the field, each pole has three holes into which 1006 (magnetic) steel rods can be inserted or removed (symmetrically in each pole) to adjust the gradient. Figure 6 shows the arrangement of those holes; Holes 1, 2, and 3 have diameters of 1.0, 2.0, and 4.75 mm, respectively, and each rod has a diameter of 0.1 mm smaller than its respective hole to aid insertion. Inserting rod 1 increases the gradient by ≈4 T/m, inserting rod 2 increases the gradient by ≈8 T/m, and inserting rod 3 increases the gradient by ≈16 T/m; thus, by the use of three rods, the gradient can be adjusted to eight different values equally spaced (in simulation) by 4 T/m. This is akin to coding a number using three binary bits, where different

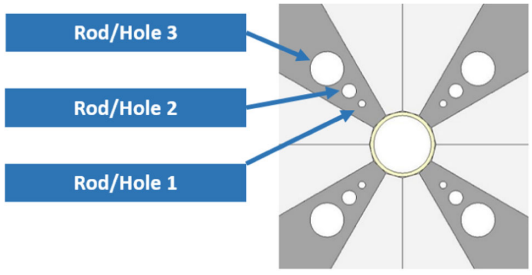


FIG. 6. Illustration of the hybrid Halbach quadrupole central region, showing the three-bit tuning holes of differing diameters (1.0, 2.0, and 4.75 mm) into which magnetic steel rods may be inserted.

TABLE III. Results of Opera-2D simulations of the eight possible insertion configurations of the three tuning rod sizes (four rods of each size), assuming symmetrical placement of four rods of a given size; the achieved variation of gradient is around 30 T/m or 6% of the total gradient. The ID number corresponds to the binary value created by a particular configuration, where rod 3 is the largest (4.75 mm), rod 2 is 2 mm, and rod 1 is 1 mm; for example, $b011 = 3$ is equivalent to OUT/IN/IN.

ID no.	Rod 3	Rod 2	Rod 1	Gradient (T/m)
0 ($b000$)	OUT	OUT	OUT	484.6
1 ($b001$)	OUT	OUT	IN	490.1
2 ($b010$)	OUT	IN	OUT	493.5
3 ($b011$)	OUT	IN	IN	498.8
4 ($b100$)	IN	OUT	OUT	502.4
5 ($b101$)	IN	OUT	IN	506.9
6 ($b110$)	IN	IN	OUT	509.9
7 ($b111$)	IN	IN	IN	514.1

bits encode different gradient changes; hence, we have dubbed it a three-bit tuning system. For a peak gradient of 500 T/m, the smallest gradient step adjustment of 4 T/m is around 0.8%, smaller than the 1% trimming accuracy required to match a set of quadrupoles together, and the total adjustment range (nearly 30 T/m or 6%) is much larger than any likely variation in remanent magnetization of the magnet blocks. This variation is confirmed through Opera-2D simulation of each tuning configuration and is shown in Table III and Fig. 7.

C. Field tolerance analysis

Using information from suppliers on the likely errors that would be expected in permanent-magnet block parameters, we assumed tolerances of ±50 μm in block dimensions, ±3% in dipole moment, and ±3° in variation of magnetization angle. One hundred randomized models were created and solved in Opera-2D [27], each sampling a uniformly distributed value over the tolerance range.

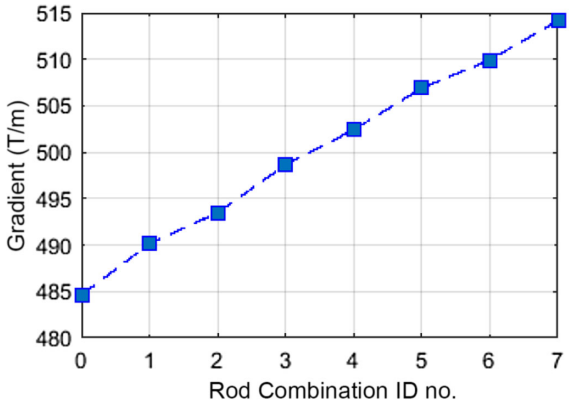


FIG. 7. Gradient vs rod combination ID No., as defined in Table III.

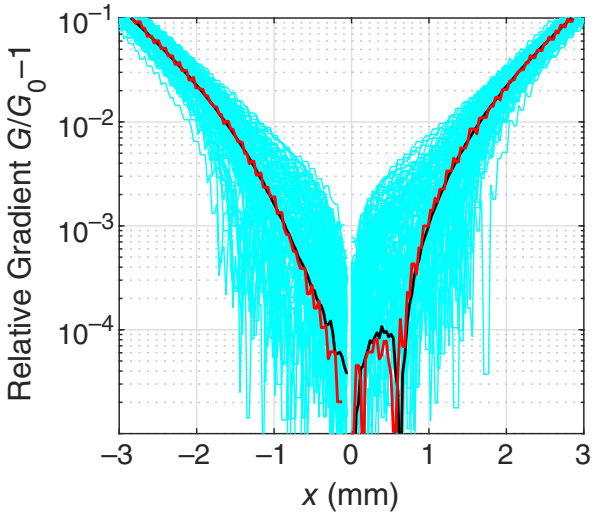


FIG. 8. Predicted gradient quality in the Halbach quadrupoles (expressed as $G/G_0 - 1$, such that 10^{-2} is a 1% gradient deviation from the desired gradient) for 100 sets of parameters randomly sampled from the likely variation of permanent-magnet block parameters; these are shown as the broad blue dataset. The mean gradient errors at a given aperture are shown as the solid lines (red for x, black for y—approximately overlying each other). These data indicate that a typical quadrupole will have a 1% gradient deviation at a radius of 1.67 mm.

Figure 8 shows that the mean 1% good gradient radius was 1.67 mm and the mean 0.1% good gradient radius was 0.93 mm; these values are consistent with the required specification shown in Table II and are confirmed by the measurements shown below.

Figure 9 predicts the full variation in gradient from the magnet block parameter tolerances to be 2.3%—much

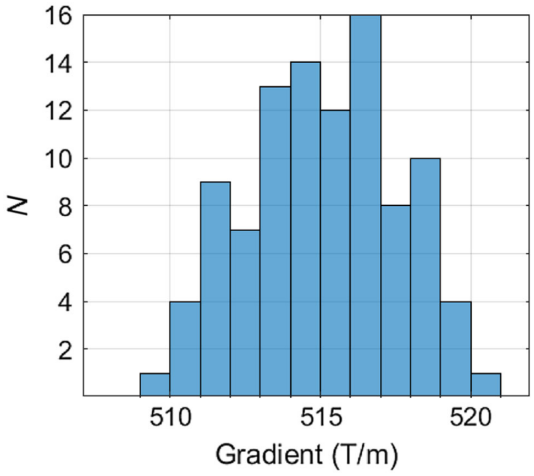


FIG. 9. Simulated distribution of predicted peak gradients in the Halbach quadrupoles due to tolerances in the permanent-magnet block parameters, estimated using 100 sets of randomly sampled parameters.

larger than 1%—confirming that gradient tuning using the three-bit method is necessary.

D. Halbach quadrupole mechanical design

The permanent-magnet blocks and steel poles are clamped within an aluminum octagonal-shaped frame which includes features for alignment and final mounting; the central beam aperture is defined with a (nonmagnetic) stainless-steel tube with outer radius of 4.5 mm and internal radius of 4.0 mm. Assembly is performed using custom assembly tooling to manage the strong forces between the poles and magnets. Each quadrupole is assembled onto a jig plate that incorporates features to aid assembly. The octagonal frame is clamped onto the jig plate and the center steel tube assembled over a dowel screwed into the jig plate. The wedge-shaped steel (AISI 1006) poles are assembled with their end pole faces in contact with the center tube, as illustrated in Fig. 10. The position and orientation of the poles are set by inserting a temporary dowel into the 4.75 mm hole in both the pole and corresponding aligning feature in the jig plate and also by the use of aluminum dummy replicate wedges in place of the magnet blocks that provide reference abutment surfaces. Adhesive is applied on the contact surfaces between the central tube and poles to secure the tube. To manage the strong forces during permanent-magnet block insertion, each magnet frame assembly is placed in a jig that allows sequential orientation of the frame for each block insertion, using an indexing pin on a jig plate. Each permanent-magnet block to be inserted is clamped into a holder attached to a hand-driven insertion guide and lead-screw; the assembly arrangement is shown in Fig. 11. The dummy wedge block is removed from the magnet assembly and replaced with a permanent-magnet block; a temporary clamp allows the assembly tooling to be removed and then

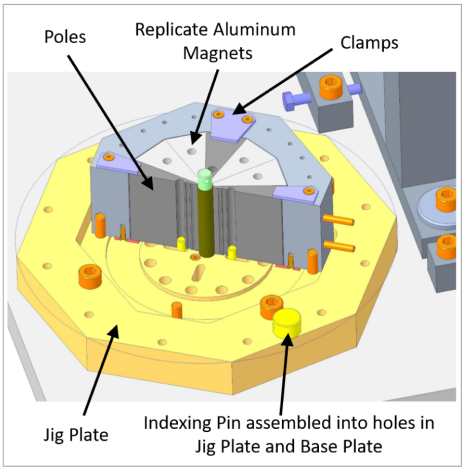


FIG. 10. Illustration of how the steel poles are assembled first into the Halbach quadrupole. Dummy aluminum replicates of the permanent-magnet blocks are used to ensure alignment.

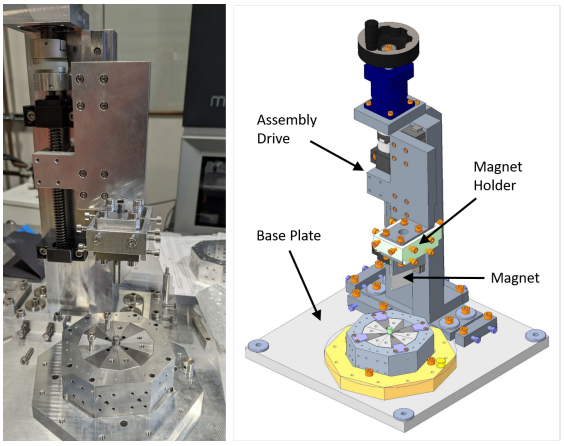


FIG. 11. Halbach quadrupole assembly (left) and diagram of assembly jig (right).

a permanent clamp is attached. This procedure is repeated for all eight magnet blocks in a prescribed order, to ensure that any opposing fields generated during block motion do not cause demagnetization of the blocks.

E. Assembly and measurement

Construction and measurement of the Halbach quadrupoles are described in a separate paper ([28]), with brief conclusions summarized here. A prototype Halbach PMQ was constructed using VACODYM-745-TP (Vacuumschmelze, Germany) as the permanent-magnet material, chosen for its high remanent flux density (1.37 T) to more readily achieve the specified 500 T/m gradient. However, this material has a somewhat lower coercivity that leads to *in situ* demagnetization of the portion of the PM blocks near the beam aperture. Optimizing the sequence of how the blocks are assembled into the PMQ limits this demagnetization such that a 360 T/m gradient can be achieved with the other magnetic parameters (field quality, harmonics etc.) remaining within specification. Future quadrupoles may utilize VACODYM-806-TP (from the same supplier) which has a somewhat lower remanent flux density of 1.3 T but high coercivity; these PMQs would then be expected to achieve over 450 T/m based on modeling of the demagnetization. Both "finished" grades of PMQ are usable in our FODO scheme since the configuration can be flexibly adjusted for different electron energies, which is equivalent to a change in PMQ gradient.

Following the prototype construction, four PMQs were constructed to form the initial capture section, and measured as shown in Table IV. These measurements confirm that the modeling of demagnetization of the prototype magnets is understood and controllable during assembly, and confirm that a suitably large good-field region can be obtained either with the present material or with another. However, the achieved 1% good-field region is somewhat smaller (at around 1.1 mm) than predicted (around 1.7 mm), but only rises slightly out to the 2 mm radius

TABLE IV. Magnetic field measurements of the first four of a series of Halbach quadrupoles. The mean achieved on-axis gradient was 360.5 T/m, as expected from modeling of the demagnetization of the material used [28]. The variation of the mean gradient of around 2% across the series is consistent with that expected from block magnetization variation, while the 1% good-field radius is somewhat smaller than predicted but still sufficient.

No.	g (T/m)	$\int gdl$ (T)	1% radius (mm)
1	360.77	18.562	1.11
2	363.94	18.763	1.18
3	357.38	18.424	1.06
4	361.421	18.643	1.01

needed for good beam transmission. The short series production of four quadrupoles also shows the limitations of relying too greatly on predictions of mean gradient, as a small sample mean has a greater likelihood of varying from the predicted mean.

Figure 12 illustrates how the capture array can be built up on three demountable plates (4/4/2 quads). This modular arrangement allows for straightforward prealignment, reconfiguration of quadrupole polarities (by rotating them by 90°). We can integrate screen diagnostics using a separate mounting rail, noting that the phase advance through the array is nearly always going to be π in each plane; phase space tomography can therefore only be partially accomplished using just these screens. Each PMQ may be moved longitudinally somewhat on its mounting plate, so having a separate mounting rail for the screens allows for convenient repositioning of the screens if necessary. Also, a tape-drive dump is situated near to the source to provide a surface at 45° to the beam direction that extracts the laser pulse at each shot.

IV. BEAMLINE DESIGN BEYOND HALBACH ARRAY

As discussed in the Introduction, unlike traditional accelerator facilities, EPAC will need a set of configurations that can be deployed in a modular fashion to serve a range of facility user experiments. For this reason, the Halbach capture array is intended to be used flexibly to assemble beamlines suitable for electrons with selectable electron energies up to 10 GeV, and to provide controllable focusing at a variable distance from the LWFA source. One option—shown in Fig. 1—gives point-to-point focusing within the source vacuum chamber at a distance of 1 m for a 1 GeV beam. This could be used, for example, to provide energy-selected laser-electron collisions for a narrow-bandwidth inverse Compton x-ray source [29]. More commonly, the beamline will include additional downstream elements to deliver the electron bunches to a diagnostic instrument or to an application. An example of an EPAC beamline configuration that we use as a design baseline is shown in Fig. 13. Here, rather than using all of the 12 possible array

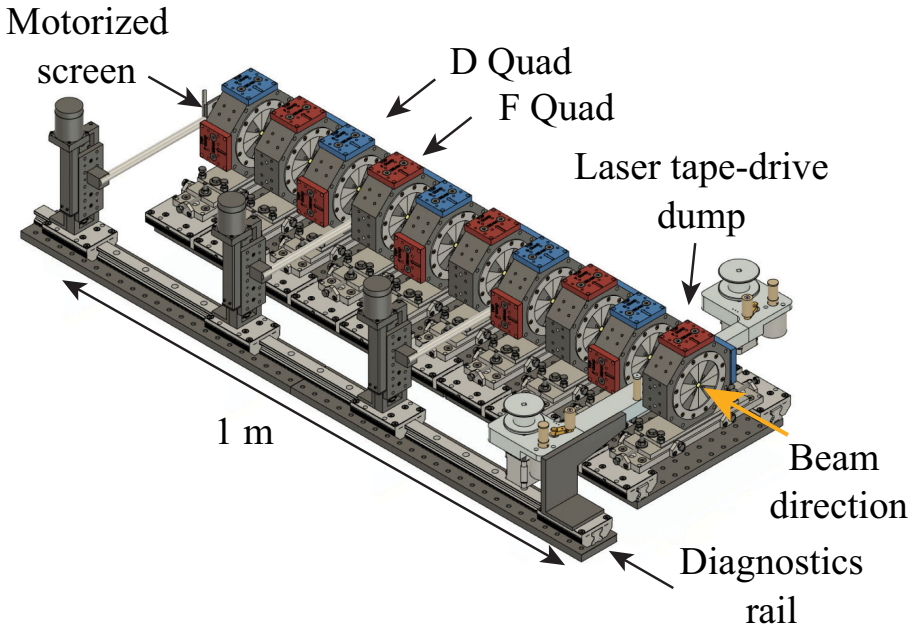


FIG. 12. Engineering illustration of a ten-quadrupole capture array that may bring a 1 GeV electron bunch to a focus within around 1 m distance. Fiducial plates (in red and blue, and on two sides of each PMQ) provide references to the quadrupole magnetic centers and allow each magnet to act as either an F or as a D quadrupole. The mounting plates allow in principle other optical configurations such as triplet or asymmetric arrangements. Individual quadrupoles will be prealigned to around 50 μm relative accuracy (to the plasma source and to each other. One possible location for the tape-drive beam dump is shown (between the first and second PMQ); also shown are the separately mounted diagnostic screens and mounting mechanisms.

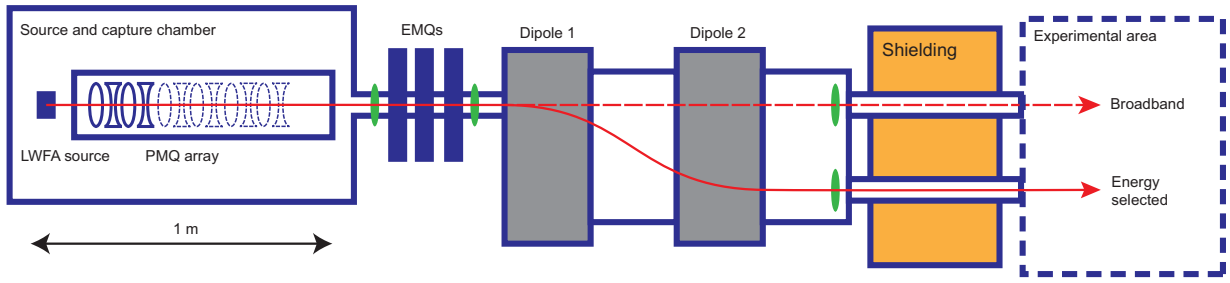


FIG. 13. Schematic of baseline 1 GeV beamline layout for EPAC EA1 (not to scale). Here, only a subset (four quadrupoles) of the PMQ capture array is used to create a beam focus some distance from the LWFA source, choosing either to transport a broadband beam or to energy-select using a two-dipole dogleg that also allows energy spectrometry to be carried out.

locations, 4 Halbach quadrupoles are employed to control the initial electron beam divergence. The electron bunches then pass through a conventional electromagnetic quadrupole (EMQ) triplet, here with a 20 mm radius internal beam aperture, that delivers more moderate adjustable gradient up to 40 T/m to provide tunable focusing.

After the focusing system, there follows a double-dipole electromagnet dogleg to measure the electron energy spectrum, similar to one proposed for SCAPA [30]. The advantage of a double-dipole design—as opposed to the simpler single dipole (such as used on AWAKE [31])—is the ability to also perform energy selection in the dispersed beam [32] and to maintain a coaxial beamline layout for applications. Furthermore, a second pair of dipoles may, in principle, be added later to create a chicane, closing the dispersion and allowing more convenient injection into a future free-electron laser [33,34]. Alternatively, by turning off the field in the dipole magnets, we can transport broadband, high-charge electron bunches directly to samples for irradiation experiments.

Obviously, the expected beam transmission will vary depending on the particular beamline and focus configuration, but, for example, with configuration A (described below), we predict a transmission of virtually all (>99%) of the entire core of the beam that lies within the 5% bandwidth around the mean energy; the halo is mostly collimated away due to its strong chromatic focusing difference with respect to the beam core.

A. Initial LWFA bunch distributions

To understand what electron focus spot sizes and beam transmission can be obtained in the EPAC beamline and to validate the electron optics design, tracking studies were carried out using two realistic representative bunch distributions; these bunch distributions were generated and optimized using FBPIC [35,36], the code chosen in part for its fast computation that allows for rapid optimization [37]. We simulated a dual-stage acceleration scheme in which the electron injection is restricted to a small region of the source; a 1 mm mixed-gas injector region is followed by a 17 mm single-gas acceleration stage [38–40]. We carried out our study with a 1 GeV central energy, which will be well within the initial capability of EPAC. These simulations used 20 J laser energy (around 2/3 of the EPAC design energy) with a pulse duration of 30 fs, corresponding to a power of about 670 TW.

FBPIC output distributions contain macroparticles of differing charges, so we resampled using a kernel density estimator (KDE) method to obtain a distribution of equal-weighted macroparticle charges for use in ELEGANT [41] tracking simulations. Examples of the electron beam distributions used in the ELEGANT tracking simulations at 1 GeV are shown in Fig. 14. We considered two configurations, optimized separately with FBPIC: a higher-charge bunch A and an alternative bunch B.

The high-charge configuration A has a relatively bright beam core surrounded by a diffuse halo that makes up the full complement of accelerated electrons; many of those halo electrons also lie significantly away from the 1 GeV central energy, in part due to their not being captured during the LWFA process, and would therefore be expected to be collimated away between the source and any downstream focal spot. Here we choose 950–1050 MeV as the bandwidth of the core bunch to be transported (as shown in Fig. 15).

The alternative configuration B is generated by optimizing parameters in FBPIC to confine all of the electrons into the smallest possible six-dimensional electron brightness [42], defined here as the full-width quarter-maximum of the distribution defined by

$$\mathcal{B}_{6D} = \frac{Q}{\gamma^2 \epsilon_{nx} \epsilon_{ny} \sigma_z \sigma_e}, \tag{1}$$

with bunch charge Q, normalized transverse emittance in the horizontal and vertical plane $\epsilon_{nx/y}$, bunch length σ_z, and energy spread σ_e. The resulting energy distribution is narrower than in configuration A.

In configuration A, the expected bunch distribution is very non-Gaussian, with a halo that includes electrons with momenta much higher and lower than the mean energy (as shown in Figs. 15 and 16). The parameters of the two configurations are given in Table V.

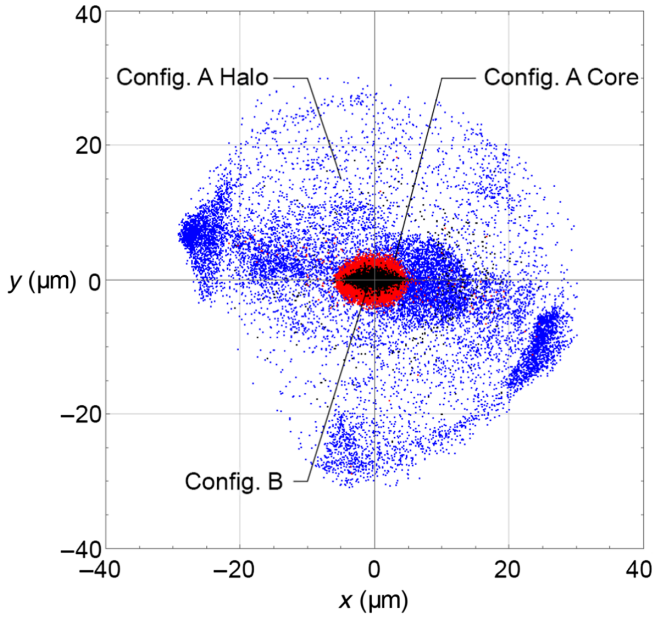


FIG. 14. FBPIC simulations showing the predicted transverse source distributions for two representative configurations in EPAC; distributions are resampled to show the equal-weight macroparticles depicted here. Configuration A gives higher charge in a central 5% bandwidth core (here shown in red depicted with its accompanying off-energy halo in blue), while configuration B (shown in black) gives a greater proportion of the total charge into a comparable emittance. The macroparticles depicted here are a subset of KDE resamples of the weighted FBPIC macroparticle output.

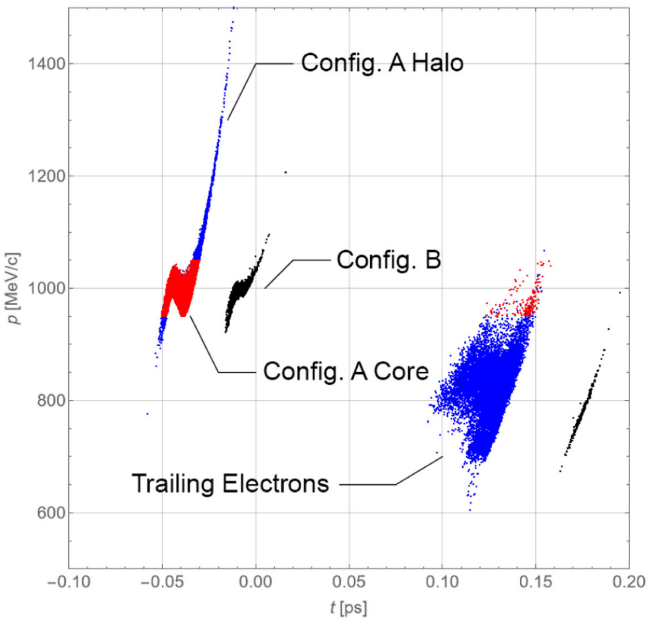


FIG. 15. FBPIC simulations showing the predicted longitudinal phase space for two representative configurations in EPAC for the same bunch configurations A (core: red and halo: blue) and B (black) shown in the previous figure.

B. Spectrometer operation

The proposed dogleg [43] comprises a pair of C-core dipole magnets with magnetic field strength up to 1.41 T, an effective length each of 0.75 m, and a longitudinal separation of 1.1 m. The operating principle is that the field strength of the two dipoles will be set to translate a desired electron energy downward by 120 mm (in other words in the y-z plane). This creates sufficient dispersion to provide $< 1\%$ energy resolution; for example, a sub-mm non-dispersive focus ($\sigma_x \approx 0.64$ mm, $\sigma_y \approx 0.50$ mm) may typically be obtained at a downstream screen location, with σ_y increasing to 3 mm when the spectrometer dipoles are set to transmit 1 GeV electrons (Fig. 17).

The dipoles have a 190 mm good-field region which provides an energy acceptance from 70% to 120% of the selected central beam energy. The integration of these dipoles into the lattice is shown in Fig. 13.

The beam size evolution of configuration A (at 1 GeV) is shown in Fig. 17. This configuration has been tuned to

TABLE V. Summary of predicted bunch properties for two representative beam configurations for EPAC, simulated using FBPIC. Configuration A yields a larger charge but has a bunch core surrounded by a significant off-energy halo; configuration B has a smaller charge but confines all of it into the same emittance.

	A			
Configuration	Full	Core	B	Unit
Mean energy	0.955	0.995	0.987	GeV
Median energy	0.989	0.996	0.999	GeV
Charge	108.00	78.96	22.56	pC
Beam size (x, y)	7.83/4.93	2.09/0.89	3.14/1.87	μm
Normalized emittance	37.19/21.19	7.24/1.38	9.00/3.00	mm mrad
Bunch length	72.0	11.4	11.6	μm
	240	38	39	fs
Relative energy spread	4.53	0.89	2.55	%

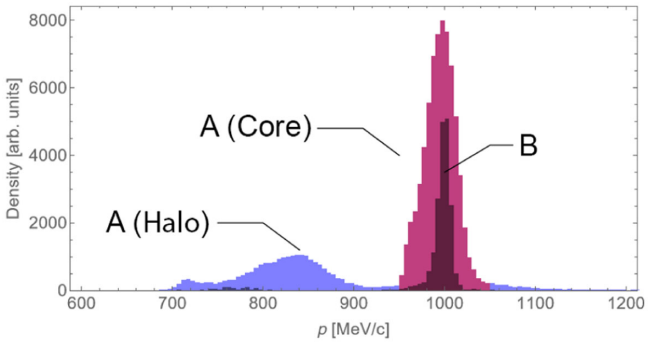


FIG. 16. FBPIC simulations as for the previous figures, showing the energy distribution of electrons exiting the LWFA source for the two representative configurations A (core: red and halo: blue) and B (black).

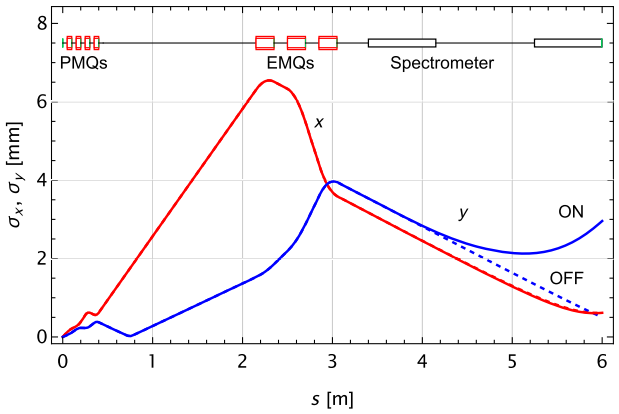


FIG. 17. Example beam size evolution in the 1 GeV baseline configuration for EPAC EA1, tuned such that the bunch is brought to a focus at a diagnostic screen; here, all particles within the central 5% bandwidth of configuration A are shown. With the spectrometer dipoles off a sub-mm focus may be achieved at the diagnostic screen (vertical in dashed, blue); with the spectrometer on, the vertical rms. Size (solid, blue) grows enough to give a 1% energy resolution leaving the horizontal size the same (red, solid).

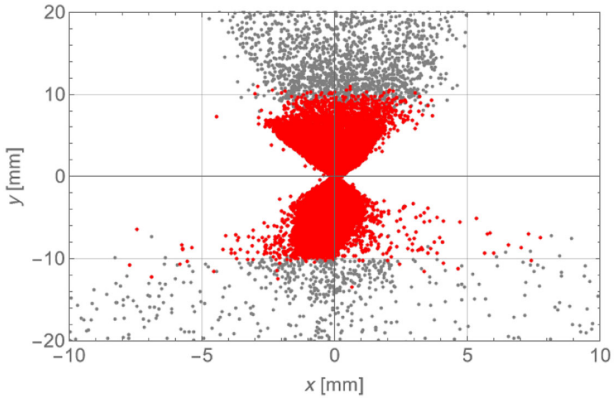


FIG. 18. Example bow tie beam from source configuration A, as calculated to be incident on a screen downstream of the spectrometer. The highlighted red particles are those that pass through the collimation; grayed particles show where those collimated in energy would strike (some losses also arise from transverse collimation in the capture section). Emittance and other parameters may be inferred by combining this profile with other beamline measurements.

achieve a small focus on the spectrometer screen located about 6 m from the LWFA source. With the dogleg dipoles energized, the dispersive component of the beam size is greater than 3 mm, which corresponds to an energy resolution of about 1%. Around 80% of the electrons are predicted to make it from the LWFA source to the screen, dominated by losses from the low-energy tail (< 700 MeV, which are collimated away throughout the beamline) and by losses of the high-energy electrons (up to 1400 MeV, which are mainly collimated away within the spectrometer). Inherent chromaticity in the focusing naturally leads to the characteristic "bow tie" expected beam shape on the spectrometer screen (see Fig. 18), that can be fitted to give a single-shot measurement of the beam emittance [44]; the greater spread of particles below $y = 0$ reflects the larger low-energy tail. The energy spread of the electron bunch gives rise to an intrinsic spreading in duration of the electron bunch as it travels from the source; this spreading will vary depending upon the optical configuration, but for example, in the case of configuration A at 1 GeV, the expected bunch duration at the spectrometer end is around 60 fs within the core of the bunch, somewhat greater than at the LWFA source.

C. Electron beam irradiation

A second option enables users to create a high-charge-density focus at varying distances along the length of the EA1 applications area. This will be used for sample irradiation experiments, such as those studying radiobiological effects [45] or to study the radiation hardness of electronics [46]. Using configuration A, we used beam tracking calculations to predict the 1 GeV beam focus that may be formed at a distance of 10 m from the LWFA source; a pair of combined horizontal/vertical trajectory correctors are to be used to assist trajectory correction. Here, the distance from PMQ array to EMQs is reduced to ameliorate unduly large beam sizes. We predict a 10 m focus size of $\sigma_x < 1$ mm, $\sigma_y < 0.5$ mm for the 5% bandwidth beam core with a transmission of over 99%, surrounded by a poorly focused off-energy halo much of which is collimated away upstream. Configuration B avoids the generation of off-energy tails but with a lower incident charge at the beam focus.

D. Adapting the beamline to higher electron energy

The advantage of our modular approach to beamline design is that we can readily increase the number of PMQ elements for high electron energies. As an example, we considered how we might deliver beamlines for 5 GeV electron energy as envisioned for the EuPRAXIA project [13]. The option of point-to-point short focal length imaging (over 2 m distance) with a pure PMQ array is achievable as described earlier, but longer-focus beamlines may be constructed with fewer quadrupoles. We modeled 5 GeV focusing to a point 15 m from the LWFA source using eight PMQs for beam conditioning and six EMQs. Again, the configuration A on-momentum electrons can be focused to a spot size less than 500 μm; beam sizes along the beamline are naturally smaller, since the initial LWFA bunch divergence scales roughly inversely with beam momentum, i.e., $\sigma' \propto 1/\gamma$. This is a promising future route to directing high-energy electron bunches from EPAC into undulator structures for x-ray generation.

E. Position tolerances of beamline elements

To establish the likely variation in achievable electron focal spot size and position, we need to know the likely variation in a number of static and dynamically changing parameters; such an analysis is also needed to know if the beamline vacuum and magnet apertures are large enough to avoid undue losses. Taking the mean LWFA laser focal position as a datum, we may align the magnetic beamline to that, and then the significant dynamic effect is that the laser focal plane position and pulse energy vary from shot to shot, giving an emerging electron bunch that varies in position and direction. The magnetic elements give a static error in that it is difficult to align the magnetic centers of the quadrupoles precisely along an intended axis, described as misalignments (Δx, Δy, Δz), and roll errors (ϕ, i.e., rotation about the beam axis); other errors have a smaller effect apart from that the PMQs will have slightly varying strengths as described earlier in this paper. We consider tolerances as shown in Table VI assigned to each of the relevant components; these values are drawn from a combination of other studies of likely parameter variations [47,48] and our own experience of constructing and positioning beamline elements.

F. Beamline error analysis

We applied the LWFA tolerances as 11 independent seeds to FBPIC simulations of the generated LWFA bunch, each seed having a focal plane and pulse energy error sampled from a normal distribution with standard deviation (σ) equal to the tolerance value but truncated at 2σ. Similarly, beamline magnetic misalignments were applied as 100 independent seeds to ELEGANT simulations with the same method of normal distribution sampling for the misalignments and FSE; the position and pointing error of the LWFA source were also sampled in the same manner. As might be expected, element misalignments mainly create position error at the downstream focus, while quadrupole strength errors mainly cause changes in the expected electron focal spot size. Taken together, the range of likely bunch centroid positions and transverse sizes dictate the required beam aperture, and we adopt the common convention of allocating a beam stay-clear (BSC) aperture that will accommodate 95% of the simulated situations (seeds). Here, we define the BSC as

$$\mathrm{BSC} = 2\Delta u_{95\%} + 2\sigma_{\mathrm{u},95\%} \tag{2}$$

with $u = x|y$, $\Delta u_{95\%}$, and $\sigma_{\mathrm{u},95\%}$ are the 95% quantile values of the trajectory and rms bunch size, respectively; a safety factor of 2 is applied. The calculated BSC is shown in Fig. 19 and confirms that a 4 mm radial aperture within the PMQs is acceptable for good transmission of the electrons.

TABLE VI. Table of tolerance values applied in the EPAC beamline error studies. LWFA source tolerances were given as 10 seeds to FBPIC simulations, and beamline tolerances were given as 100 seeds to ELEGANT bunch tracking simulations.

Tolerance	Value	Unit
LWFA source		
Laser focal plane position	±2	mm
Laser pulse energy	±2.5	%
Beamline		
Initial bunch position error	±100	μm
Initial bunch pointing error	±10	μrad
PMQ transverse misalignment	±50	μm
PMQ fractional strength error (FSE)	±1	%

G. LWFA source and beamline error analysis

Errors from the LWFA source such as variations in the laser pulse energy, laser longitudinal focal plane position and gas density will modify the trajectory and beam size of the electron beam. Using the tolerance values above, 11 sampled bunches were each tracked 10 times through different randomly sampled beamline errors. The resulting beam sizes are shown in Fig. 20. From these estimates, we see that the larger contribution to beam size variation is PMQ errors—around 100 μm—with around 50 μm from pointing variation of the source; the large horizontal values are due to the effect of the laser polarization driving the plasma generation. Conversely, and unsurprisingly, the initial pulse-by-pulse variation in the bunch pointing leads to a fluctuation in source position at the focal point of about 250 μm. This implies that beam-based alignment of the quadrupoles to a common axis should reduce the achievable focal spot size variation to 50 μm, i.e., that caused by

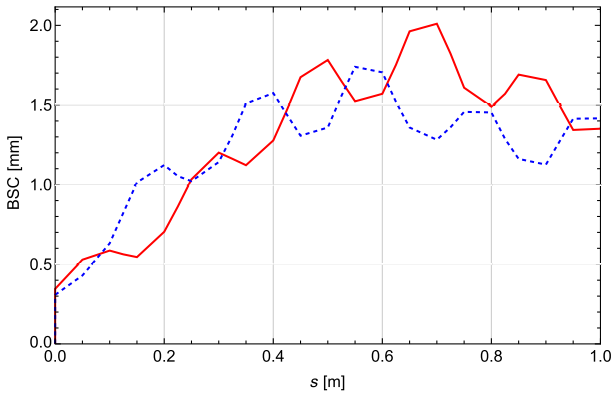


FIG. 19. Beam stay clear [Eq. (2)] at 1 GeV within the PMQ array, for the 1 GeV point-to-point focusing 1 m from the LWFA source; note, in particular, the larger downstream required BSC due to a combination of initial laser pointing error and PMQ misalignment. The horizontal BSC is shown as a solid line (red), the vertical BSC is shown as a dashed line (blue).

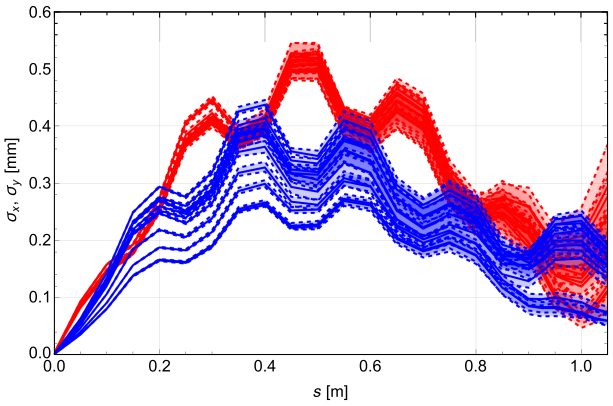


FIG. 20. Variation in actual predicted beam sizes (red showing horizontal, blue showing vertical) through the 1 GeV point-to-point ten-quadrupole configuration caused by variation in source and beamline parameters, calculated from 11 bunch seed samples (from FBPIC simulations), each tracked through 10 beamline samples using ELEGANT. The BSC in the previous figure is derived from a 95% confidence interval of a number of these calculations using Eq. (2), and is depicted in this figure as the shaded region.

source fluctuation. Similar conclusions can be made for the other beamline configurations, but this will have to be shown in later experimental measurements.

The predicted level of shot-to-shot fluctuation can be tolerated for some applications that will be served by EPAC. For example, radiation hardness testing of materials and electronics will typically irradiate a mm-scale area at a meter-scale distance from the source; in this case, maximizing the charge delivered to the sample is more important than precise beam alignment. However, for configurations where alignment is critical—such as colliding with a second laser focus for inverse Compton scattering—more sophisticated stabilization routines will need to be developed [47,48].

V. CONCLUSIONS

We have developed the design of a novel modular, tunable beamline for laser-accelerated electron bunches using a PMQ array for beam conditioning, which allows simple reconfiguration for different electron energies and experimental situations; we expect that this concept will be useful for other LWFA facilities. To achieve uniformity of the PMQs, we have presented a new tuning pin method and have demonstrated it with a prototype. We show a robust mounting and adjustment concept that will allow sufficient alignment to be achieved to maintain good beam quality and transmission to be preserved through beam transport; a comprehensive error analysis supports this. We intend to construct this beamline in stages over the next 2 years, beginning with a four-quadrupole configuration to support early experimentation on EPAC.

DATA AVAILABILITY

The data that support the findings of this article are openly available [49], embargo periods may apply.

[1] E. Esarey, C. B. Schroeder, and W. P. Leemans, Physics of laser-driven plasma-based electron accelerators, Rev. Mod. Phys. **81**, 1229 (2009).

[2] P. D. Mason, S. Banerjee, K. Ertel, P. J. Phillips, T. J. Butcher, J. M. Smith, M. D. Vido, S. Tomlinson, O. Chekhlov, W. Shaikh, S. Blake, P. Holligan, M. Divoky, J. Pilar, C. Hernandez-Gomez, J. Greenhalgh, and J. L. Collier, DiPOLE100: A 100 J, 10 Hz DPSSL using cryogenic gas cooled Yb:YAG multi slab amplifier technology, in *High-Power, High-Energy, and High-Intensity Laser Technology II*, edited by J. Hein (International Society for Optics and Photonics-SPIE, 2015), Vol. 9513, p. 951302.

[3] L. McHugh, D. Clarke, P. Mason, R. Heathcote, J. Phillips, M. Harman, S. Tomlinson, T. Butcher, C. Hernandez-Gomez, and J. Collier, Commissioning a high-energy 10 Hz Ti:Sa amplifier for the petawatt laser at the extreme photonics applications centre, in *Solid State Lasers XXXIV: Technology and Devices*, edited by W. A. Clarkson and R. K. Shori (International Society for Optics and Photonics-SPIE, 2025), Vol. 13341, p. 133410A.

[4] C. M. S. Sears, A. Buck, K. Schmid, J. Mikhailova, F. Krausz, and L. Veisz, Emittance and divergence of laser wakefield accelerated electrons, Phys. Rev. ST Accel. Beams **13**, 092803 (2010).

[5] B. Hidding, A. Beaton, L. Boulton, S. Corde, A. Doepp, F. A. Habib, T. Heinemann, A. Irman, S. Karsch, G. Kirwan, A. Knetsch, G. G. Manahan, A. Martinez de la Ossa, A. Nutter, P. Scherkl, U. Schramm, and D. Ullmann, Fundamentals and applications of hybrid LWFA-PWFA, Appl. Sci. **9**, 2626 (2019).

[6] A. Loulergue, M. Labat, C. Evain, C. Benabderrahmane, V. Malka, and M. E. Couprie, Beam manipulation for compact laser wakefield accelerator based free-electron lasers, New J. Phys. **17**, 023028 (2015).

[7] S. Jalas, M. Kirchen, C. Braun, T. Eichner, J. B. Gonzalez, L. Hübner, T. Hülsenbusch, P. Messner, G. Palmer, M. Schnepp, C. Werle, P. Winkler, W. P. Leemans, and A. R. Maier, Tuning curves for a laser-plasma accelerator, Phys. Rev. Accel. Beams **26**, 071302 (2023).

[8] F. Irshad, C. Eberle, F. M. Foerster, K. v. Grafenstein, F. Haberstroh, E. Travac, N. Weisse, S. Karsch, and A. Döpp, Pareto optimization and tuning of a laser wakefield accelerator, Phys. Rev. Lett. **133**, 085001 (2024).

[9] C. Aniculaesei *et al.*, The acceleration of a high-charge electron bunch to 10 GeV in a 10-cm nanoparticle-assisted wakefield accelerator, Matter Radiat. Extremes **9**, 014001 (2023).

[10] A. J. Gonsalves *et al.*, Petawatt laser guiding and electron beam acceleration to 8 GeV in a laser-heated capillary discharge waveguide, Phys. Rev. Lett. **122**, 084801 (2019).

[11] A. Picksley, J. Stackhouse, C. Benedetti, K. Nakamura, H. E. Tsai, R. Li, B. Miao, J. E. Shrock, E. Rockafellow, H. M. Milchberg, C. B. Schroeder, J. van Tilborg, E.

Esarey, C. G. R. Geddes, and A. J. Gonsalves, Matched guiding and controlled injection in dark-current-free, 10-GeV-class, channel-guided laser-plasma accelerators, Phys. Rev. Lett. **133**, 255001 (2024).

[12] T. Levato *et al.*, Hell: High-energy electrons by laser light, a user-oriented experimental platform at ELI beamlines, Appl. Sci. **8**, 1565 (2018).,

[13] R. Assmann, M. Weikum, T. Akhter, D. Alesini, A. Alexandrova, M. Anania, N. Andreev, I. Andriyash, M. Artioli, A. Aschikhin *et al.*, EuPRAXIA conceptual design report, Eur. Phys. J. Special Topics **229**, 3675 (2020).

[14] G. Hoffstaetter and R. Ryan, Small accelerator promises big returns, CERN Courier **58**, 19 (2018), https://cerncourier.com/a/small-accelerator-promises-big-returns/.

[15] D. Trbojevic *et al.*, CBETA—Cornell University Brookhaven National Laboratory Electron Energy Recovery Test Accelerator, in *Proceedings of the 8th International Particle Accelerator Conference, IPAC-2017, Copenhagen, Denmark* (JACoW, Geneva, Switzerland, 2017), pp. 1285–1289, 10.18429/JACoW-IPAC2017-TUOCB3.

[16] G. H. Hoffstaetter *et al.*, CBETA design report, Cornell-BNL ERL Test Accelerator, arXiv:1706.04245.

[17] D. Trbojevic *et al.*, A novel use of FFAGs in ERLs—in colliders: eRHIC, LHeC and a prototype at Cornell University, in *Proceedings of the 21st International Conference on Cyclotrons and Their Applications, Cyclotrons 2016, Zurich, Switzerland* (JACoW, Geneva, Switzerland, 2016), pp. 140–144.

[18] D. Trbojevic, S. Brooks, W. Lou, B. Parker, and N. Tsoupas, Permanent Halbach magnet proton and superconducting carbon cancer therapy gantries, in *Proceedings of the 8th International Particle Accelerator Conference, IPAC-2017, Copenhagen, Denmark* (JACoW, Geneva, Switzerland, 2017), pp. 4679–4682, 10.18429/JACoW-IPAC2017-THPVA094.

[19] N. Tsoupas *et al.*, The beam optics of the FFAG cell of the CBETA ERL accelerator, in *Proceedings of the 8th International Particle Accelerator Conference, IPAC-2017, Copenhagen, Denmark* (JACoW, Geneva, Switzerland, 2017), pp. 820–823, 10.18429/JACoW-IPAC2017-MOPIK122.

[20] J. van Tilborg, S. Steinke, C. G. R. Geddes, N. H. Matlis, B. H. Shaw, A. J. Gonsalves, J. V. Huijts, K. Nakamura, J. Daniels, C. B. Schroeder, C. Benedetti, E. Esarey, S. S. Bulanov, N. A. Bobrova, P. V. Sasorov, and W. P. Leemans, Active plasma lensing for relativistic laser-plasma-accelerated electron beams, Phys. Rev. Lett. **115**, 184802 (2015).

[21] J. A. Clarke, N. A. Collomb, B. J. Shepherd, D. G. Stokes, A. Bartalesi, M. Modena, and M. Struik, Novel tunable permanent magnet quadrupoles for the CLIC drive beam, IEEE Trans. Appl. Supercond. **24**, 1 (2013).

[22] B. Shepherd, J. Clarke, N. Marks, N. Collomb, D. Stokes, M. Modena, M. Struik, and A. Bartalesi, Tunable high-gradient permanent magnet quadrupoles, J. Instrum. **9**, T11006 (2014).

[23] F. Marteau, A. Ghaith, P. N'Gotta, C. Benabderrahmane, M. Valléau, C. Kitegi, A. Loulergue, J. Vétéran, M. Sebdaoui, T. André, G. Le Bec, J. Chavanne, C. Vallerand, D. Oumbarek, O. Cosson, F. Forest, P. Jivkov, J. L. Lancelot, and M. E. Couprie, Variable high gradient permanent magnet quadrupole (QUAPEVA), Appl. Phys. Lett. **111**, 253503 (2017).

[24] P. Antici, A. Bacci, C. Benedetti, E. Chiadroni, M. Ferrario, A. Rossi, L. Lancia, M. Migliorati, A. Mostacci, L. Palumbo *et al.*, Laser-driven electron beamlines generated by coupling laser-plasma sources with conventional transport systems, J. Appl. Phys. **112**, 044902 (2012).

[25] R. Pompili, M. Anania, E. Chiadroni, A. Cianchi, M. Ferrario, V. Lollo, A. Notargiacomo, L. Picardi, C. Ronsivalle, J. Rosenzweig *et al.*, Compact and tunable focusing device for plasma wakefield acceleration, Rev. Sci. Instrum. **89**, 033302 (2018).

[26] B. Muratori, J. Jones, K. Dewhurst, and H. Owen, High acceptance beamline for the capture of a laser wakefield accelerated beam, in *Proceedings of the 9th International Particle Accelerator Conference, IPAC-2018, Vancouver, BC, Canada* (JACoW, Geneva, Switzerland, 2018), pp. 3456–3459.

[27] 3DS, Opera simulation software, http://www.3ds.com/products/simulia/opera [accessed on January 9, 2025].

[28] A. Bainbridge, A. Hinton, C. Hill, T. Smith, B. Pine, and N. Thompson, Measurement and simulation of demagnetization in a prototype Halbach array quadrupole, Metrology **5**, 15 (2025).

[29] T. Brümmer, S. Bohlen, F. Grüner, J. Osterhoff, and K. Põder, Compact all-optical precision-tunable narrowband hard Compton x-ray source, Sci. Rep. **12**, 16017 (2022).

[30] A. Maitrallain, B. van der Geer, M. de Loos, G. Manahan, S. M. Wiggins, W. Li, M. Shahzad, R. Spesyvtsev, G. Battaglia, G. Vieux *et al.*, Design of a double dipole electron spectrometer, in *Laser Acceleration of Electrons, Protons, and Ions V* (SPIE, 2019), Vol. 11037, pp. 80–89.

[31] F. Keeble *et al.*, The AWAKE electron spectrometer, in *Proceedings of the 9th International Particle Accelerator Conference, IPAC-2018, Vancouver, BC, Canada* (JACoW, Geneva, Switzerland, 2018), pp. 4947–4950, 10.18429/JACoW-IPAC2018-THPML118.

[32] T. André *et al.*, Control of laser plasma accelerated electrons for light sources, Nat. Commun. **9**, 1334 (2018).

[33] A. R. Maier, A. Meseck, S. Reiche, C. B. Schroeder, T. Seggebrock, and F. Grüner, Demonstration scheme for a laser-plasma-driven free-electron laser, Phys. Rev. X **2**, 031019 (2012).

[34] M. Labat *et al.*, Seeded free-electron laser driven by a compact laser plasma accelerator, Nat. Photonics **17**, 150 (2023).

[35] R. Lehe, M. Kirchen, S. Jalas, K. Peters, and I. Dornmair, Fourier-Bessel Particle-In-Cell (FBPIC) v0. 1.0, Technical Report, Lawrence Berkeley National Laboratory (LBNL), Berkeley, CA, 2017.

[36] M. Kirchen, S. Jalas, S. Mahncke, and A. R. Maier, FBPIC: A spectral, quasi-3D, multi-GPU particle-in-cell code for plasma accelerators, Verh. Dtsch. Phys. Ges. (2018), https://www.dpg-verhandlungen.de/year/2018/conference/wuerzburg/part/akbp/session/8/contribution/11.

[37] S. Jalas, M. Kirchen, P. Messner, P. Winkler, L. Hübner, J. Dirkwinkel, M. Schnepp, R. Lehe, and A. R. Maier, Bayesian optimization of a laser-plasma accelerator, Phys. Rev. Lett. **126**, 104801 (2021).

[38] A. Pak, K. A. Marsh, S. F. Martins, W. Lu, W. B. Mori, and C. Joshi, Injection and trapping of tunnel-ionized electrons into laser-produced wakes, Phys. Rev. Lett. **104**, 025003 (2010).

[39] C. McGuffey, A. G. R. Thomas, W. Schumaker, T. Matsuoka, V. Chvykov, F. J. Dollar, G. Kalintchenko, V. Yanovsky, A. Maksimchuk, K. Krushelnick, V. Y. Bychenkov, I. V. Glazyrin, and A. V. Karpeev, Ionization induced trapping in a laser wakefield accelerator, Phys. Rev. Lett. **104**, 025004 (2010).

[40] J. S. Liu, C. Q. Xia, W. T. Wang, H. Y. Lu, C. Wang, A. H. Deng, W. T. Li, H. Zhang, X. Y. Liang, Y. X. Leng, X. M. Lu, C. Wang, J. Z. Wang, K. Nakajima, R. X. Li, and Z. Z. Xu, All-optical cascaded laser wakefield accelerator using ionization-induced injection, Phys. Rev. Lett. **107**, 035001 (2011).

[41] M. Borland, ELEGANT: A flexible SDDS-compliant code for accelerator simulation, Technical Report LS-287, Argonne National Laboratory, Illinois, 2000.

[42] S. Di Mitri, On the importance of electron beam brightness in high gain free electron lasers, in *Photonics* (MDPI, Basel, Switzerland, 2015), Vol. 2, pp. 317–341, 10.3390/photonics2020317.

[43] A. Bainbridge, J. Crone, J. Jones, B. Muratori, H. Owen, T. Pacey, B. Shepherd, D. Angal-Kalinin, D. Symes, and N. Bourgeois, Design of an electron energy spectrometer and energy selector for laser-plasma driven beams at EPAC, in *Proceedings of the 14th International Particle Accelerator Conference, IPAC-2023, Venice, Italy* (JACoW, Geneva, Switzerland, 2023), pp. 4568–4571.

[44] S. K. Barber, J. van Tilborg, C. B. Schroeder, R. Lehe, H.-E. Tsai, K. K. Swanson, S. Steinke, K. Nakamura, C. G. R. Geddes, C. Benedetti, E. Esarey, and W. P. Leemans, Measured emittance dependence on the injection method in laser plasma accelerators, Phys. Rev. Lett. **119**, 104801 (2017).

[45] L. Labate, D. Palla, D. Panetta, F. Avella, F. Baffigi, F. Brandi, F. Di Martino, L. Fulgentini, A. Giulietti, P. Köster, D. Terzani, P. Tomassini, C. Traino, and L. A. Gizzi, Toward an effective use of laser-driven very high energy electrons for radiotherapy: Feasibility assessment of multi-field and intensity modulation irradiation schemes, Sci. Rep. **10**, 17307 (2020).

[46] B. Hidding, T. Königstein, O. Willi, J. B. Rosenzweig, K. Nakajima, and G. Pretzler, Laser–plasma-accelerators—A novel, versatile tool for space radiation studies, Nucl. Instrum. Methods Phys. Res., Sect. A **636**, 31 (2011).

[47] C. Berger, S. Barber, F. Isono, K. Jensen, J. Natal, A. Gonsalves, and J. van Tilborg, Active nonperturbative stabilization of the laser-plasma-accelerated electron beam source, Phys. Rev. Accel. Beams **26**, 032801 (2023).

[48] A. Amodio, D. Wang, C. Berger, H.-E. Tsai, S. K. Barber, J. van Tilborg, A. Picksley, Z. Eisentraut, N. R. Vora, M. Logantha *et al.*, Pointing stabilization of a 1 Hz high-power laser via machine learning, High Power Laser Sci. Eng. **13**, e35 (2025).

[49] B. Muratori, D. Angal-Kalinin, A. Bainbridge, J. Crone, C. Hill, J. Jones, H. Owen, T. Pacey, Y. Saveliev, N. Thompson, D. Symes, N. Bourgeois, and O. Finlay, STFC eData Repository (2026), 10.5286/edata/967.